Machine Copy for Proofreading, Vol. x, y–z, 2012

EVALUATION OF THE FAR FIELD RADIATED BY LONG ANTENNAS DIRECTLY FROM DATA ACQUIRED THROUGH A FAST HELICOIDAL SCANNING

F. D'Agostino, F. Ferrara, C. Gennarelli*, R. Guerriero, and M. Migliozzi

Dipartimento di Ingegneria Elettronica e Ingegneria Informatica, University of Salerno, via Ponte Don Melillo, Fisciano, Salerno 84084, Italy

Abstract—A direct near-field-far-field transformation with helicoidal scanning for electrically long antennas is proposed in this paper. Such a transformation, which allows the evaluation of the antenna far field in any cut plane directly from the acquired near-field data without interpolating them, relies on the nonredundant sampling representation of electromagnetic fields and makes use of a prolate ellipsoidal modelling of the antenna under test for determining the number of helix turns, whereas the number of samples on each of them is fixed by the minimum cylinder rule, as in the classical cylindrical scan. Numerical and experimental tests assessing the effectiveness of the approach are shown.

1. INTRODUCTION

Many efforts have been spent in the recent years to reduce the time required for the near-field data acquisition, since this time is currently very much greater than that needed to carry out the near-field-far-field (NF-FF) transformation. Such a reduction can be realized by reducing the number of data to be collected and/or making faster their acquisition. In this framework, the nonredundant sampling representations of electromagnetic (EM) fields [1] have been profitably applied to develop NF-FF transformations with planar, cylindrical and spherical scannings [2], which generally require a number of NF data remarkably lower than the standard ones. In fact, the NF data needed by the corresponding classical NF-FF transformations are accurately recovered by interpolating the

Received 20 September 2012.

* Corresponding author: Claudio Gennarelli (gennar@diiie.unisa.it).

minimum set of measurements via optimal sampling interpolation (OSI) formulas [3]. A considerable measurement time saving can be then obtained by exploiting continuous and synchronized movements of the positioning systems of the probe and antenna under test (AUT) [4]. This suggestion has allowed the development of innovative NF-FF transformations with helicoidal scanning [5–10], and planar [6, 7, 11, 12] and spherical [6, 7, 13–15] spiral scannings. They are based on the aforementioned nonredundant representations and use a proper two-dimensional OSI algorithm to reconstruct the NF data needed by the corresponding classical NF-FF transformation technique. The OSI expansion has been achieved: i) by assuming the AUT enclosed in a proper convex domain bounded by a surface Σ with rotational symmetry; ii) by developing a nonredundant sampling representation of the voltage acquired by the probe on the spiral; iii) by choosing the spiral step equal to the sample spacing required for interpolating the NF data along a meridian curve (a generatrix in the helicoidal scanning, a radial line and a meridian in the planar and spherical scanning, respectively).

With reference to the NF-FF transformation with helicoidal scanning, which is particularly attractive when dealing with antennas that concentrate the EM radiation in an angular region centred on the horizontal plane, the AUT has been considered as enclosed in the smallest sphere able to contain it in [5, 6], whereas more effective AUT modellings, allowing a further reduction of the required NF data in the case of elongated antennas, have been adopted in [8–10] by properly employing the unified theory of spiral scans for nonspherical antennas [7]. These effective AUT modellings allow one to consider measurement cylinders with a radius smaller than one half the antenna maximum size, thus reducing the error due to the truncation of the scanning zone. More in detail, an elongated AUT has been considered as enclosed in a prolate ellipsoid in [8, 9] or in a cylinder ended in two half spheres in [10].

A probe uncompensated NF-FF transformation with helicoidal scanning has been proposed in [16] to efficiently determine the antenna far field directly from the acquired helicoidal NF data. It employs a fast Fourier transform (FFT) based algorithm to evaluate the antenna far field without requiring any interpolation step. However, since such an approach does not take advantage of the nonredundant representations of EM fields, it needs a useless large amount of NF data.

On the contrary, a direct NF-FF transformation with cylindrical scanning for long antennas, based on the aforementioned nonredundant sampling representations and using a prolate ellipsoidal modelling, has been proposed in [17] and experimentally assessed in [18]. It allows

the evaluation of the antenna far field in any cut plane directly from the nonredundant NF data without interpolating them. Moreover, it exhibits the interesting property to eliminate the characteristic ripple due to the discontinuity of the near field at the edges of the scanning zone.

At last, in order to match the advantages of the direct cylindrical NF-FF transformation with those characteristic of the helicoidal scanning, a direct NF-FF transformation technique with helicoidal scanning for volumetrical antennas has been recently proposed in [19]. Unfortunately, this last is not suitable for electrically long antennas, since it employs the spherical AUT modelling.

The aim of this paper is to develop and validate, both numerically and experimentally, a direct NF-FF transformation with helicoidal scanning tailored for elongated antennas. In particular, the number of helix turns is fixed by the nonredundant sampling representation along a generatrix, obtained when adopting the prolate ellipsoidal modelling of the AUT, whereas the number of samples on each of them is determined by the AUT maximum transverse dimension to simplify the mechanical scanning and to reduce the computational effort.

2. THEORETICAL BACKGROUND

For reader's convenience, the key steps of the classical probe compensated NF-FF transformation with cylindrical scanning [20], as well as those relevant to the reconstruction of the probe voltage from a nonredundant number of its samples lying along a helix [8], are summarized in this section.

2.1. Classical NF-FF Transformation with Cylindrical Scanning

Let us consider a probe scanning a cylinder of radius d in the antenna NF region, and adopt the cylindrical coordinate system $(\rho,\ \varphi,\ z)$ to denote an observation point in the NF region. According to the classical probe compensated NF-FF transformation with cylindrical scanning [20], the modal coefficients a_ν and b_ν of the cylindrical wave expansion of the field radiated by the AUT are related to: a) the two-dimensional Fourier transforms I_ν^1 and I_ν^2 of the output voltages of the probe for two independent sets of measurements (the probe is rotated 90° about its longitudinal axis in the second set); b) the coefficients $(c_m,\ d_m)$ and $(c'_m,\ d'_m)$ of the cylindrical wave expansion of the field radiated by the probe and the rotated probe, respectively, when used

as transmitting antennas. The key relations [20] are:

$$a_\nu(\tau) = \frac{\beta^2}{\Lambda^2 \Delta_\nu(\tau)} \left[I_\nu^1(\tau) \sum_{m=-\infty}^{\infty} d'_m(-\tau) H_{\nu+m}^{(2)}(\Lambda d) - I_\nu^2(\tau) \sum_{m=-\infty}^{\infty} d_m(-\tau) H_{\nu+m}^{(2)}(\Lambda d) \right] \quad (1)$$

$$b_\nu(\tau) = \frac{\beta^2}{\Lambda^2 \Delta_\nu(\tau)} \left[I_\nu^2(\tau) \sum_{m=-\infty}^{\infty} c_m(-\tau) H_{\nu+m}^{(2)}(\Lambda d) - I_\nu^1(\tau) \sum_{m=-\infty}^{\infty} c'_m(-\tau) H_{\nu+m}^{(2)}(\Lambda d) \right] \quad (2)$$

$$\Delta_\nu(\tau) = \sum_{m=-\infty}^{\infty} c_m(-\tau) H_{\nu+m}^{(2)}(\Lambda d) \sum_{m=-\infty}^{\infty} d'_m(-\tau) H_{\nu+m}^{(2)}(\Lambda d) - \sum_{m=-\infty}^{\infty} c'_m(-\tau) H_{\nu+m}^{(2)}(\Lambda d) \sum_{m=-\infty}^{\infty} d_m(-\tau) H_{\nu+m}^{(2)}(\Lambda d) \quad (3)$$

$$I_\nu^{1,2}(\tau) = \int_{-\infty}^{\infty} \int_{-\pi}^{\pi} V^{1,2}(\varphi, z)\, e^{-j\nu\varphi} e^{j\tau z}\, d\varphi\, dz \quad (4)$$

wherein $\Lambda = (\beta^2 - \tau^2)^{1/2}$, $H_\nu^{(2)}(\cdot)$ is the Hankel function of second kind and order ν, β is the wavenumber, and V^1, V^2 are the output voltages of the probe and the rotated probe at the point of cylindrical coordinates (d, φ, z).

Note that the Fourier transforms (4) of the probe and rotated probe voltages can be efficiently evaluated via the FFT algorithm. Moreover, the sample spacings of the NF data are $\Delta z \leq \lambda/2$ and $\Delta\varphi \leq \pi/(\beta\rho') = \lambda/(2\rho')$, where ρ' is the radius of the smallest cylinder enclosing the AUT (minimum cylinder rule) and λ is the wavelength.

Once the modal coefficients a_ν and b_ν have been determined, the FF spherical components of the electric field in the spherical coordinate system (r, ϑ, φ) can be efficiently evaluated by performing the summations in the following relations via FFT:

$$E_\vartheta(r,\vartheta,\varphi) = F_\vartheta(\vartheta,\varphi) \frac{e^{-j\beta r}}{r} = -j2\beta \frac{e^{-j\beta r}}{r} \sin\vartheta \sum_{\nu=-\infty}^{\infty} j^\nu b_\nu(\beta\cos\vartheta)\, e^{j\nu\varphi} \quad (5)$$

$$E_\varphi(r,\vartheta,\varphi) = F_\varphi(\vartheta,\varphi) \frac{e^{-j\beta r}}{r} = -2\beta \frac{e^{-j\beta r}}{r} \sin\vartheta \sum_{\nu=-\infty}^{\infty} j^\nu a_\nu(\beta\cos\vartheta)\, e^{j\nu\varphi} \quad (6)$$

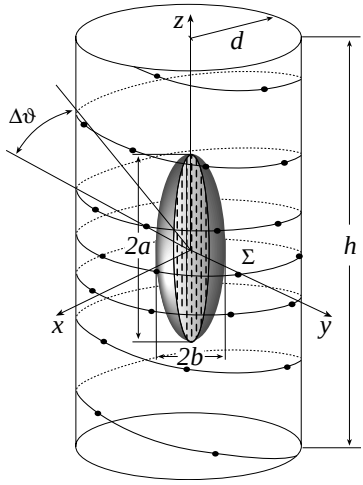

Figure 1. Helicoidal scanning: prolate ellipsoidal modelling.

2.2. Nonredundant Sampling Representation on a Cylinder

Let us consider an elongated AUT, enclosed in a convex domain bounded by a surface Σ with rotational symmetry, and a nondirective probe scanning a proper helix lying on a cylinder of radius d in the NF region. An effective modelling for such a kind of AUT is obtained by choosing Σ coincident with a prolate ellipsoid having major and minor semi-axes equal to a and b (Figure 1). Since the voltage measured by a nondirective probe has the same effective spatial bandwidth of the AUT field [21], the nonredundant representations of EM fields [1] can be applied to it. Accordingly, in order to obtain the representation of the probe voltage on an observation curve C, it is convenient to adopt an optimal analytical parameterization $\underline{r} = \underline{r}(\eta)$ to describe C and to introduce the "reduced voltage"

$$\tilde{V}(\eta) = V(\eta)e^{j\psi(\eta)}, \tag{7}$$

where $V(\eta)$ is the measured probe voltage, $\psi(\eta)$ is a proper phase function, and η is an optimal parameter used to describe C. The bandlimitation error, occurring when $\tilde{V}(\eta)$ is approximated by a spatially bandlimited function, becomes negligible as the bandwidth exceeds a critical value W_η [1], so that it can be effectively controlled by choosing a bandwidth equal to $\chi' W_\eta$, where $\chi' > 1$ is the bandwidth enlargement factor.

According to [7, 8], a two-dimensional OSI scheme to reconstruct the voltage from a nonredundant number of its samples collected

by the probe along a helix can be obtained: a) by developing a nonredundant sampling representation of the probe voltage on the helix; b) by choosing the helix step equal to the sample spacing required to interpolate the data along a generatrix. In particular, the bandwidth W_η and parameterization η relevant to a generatrix, and the corresponding phase function ψ are [7, 8]:

$$W_\eta = (4a/\lambda)\, E\left(\pi/2 \,|\, \varepsilon^2\right), \tag{8}$$

$$\eta = (\pi/2)\left[1 + E\left(\sin^{-1} u \,|\, \varepsilon^2\right)/E\left(\pi/2 \,|\, \varepsilon^2\right)\right], \tag{9}$$

$$\psi = \beta a \left[v\sqrt{\frac{v^2-1}{v^2-\varepsilon^2}} - E\left(\cos^{-1}\sqrt{\frac{1-\varepsilon^2}{v^2-\varepsilon^2}}\,|\varepsilon^2\right)\right], \tag{10}$$

where $u = (r_1 - r_2)/2f$ and $v = (r_1 + r_2)/2a$ are the elliptic coordinates, $r_{1,2}$ being the distances from observation point P to the foci of the ellipse C', intersection curve between a meridian plane and Σ, and $2f$ is the focal distance. Moreover, $\varepsilon = f/a$ is the eccentricity of C' and $E\,(\cdot|\cdot)$ denotes the elliptic integral of second kind.

The parametric equations of the helix, when imposing its passage through a fixed point Q_0 of the generatrix at $\varphi = 0$, are:

$$\begin{cases} x = d\cos(\phi - \phi_s) \\ y = d\sin(\phi - \phi_s) \\ z = d\cot[\vartheta(\eta)] \end{cases}, \tag{11}$$

wherein ϕ is the parameter describing the helix, ϕ_s is the value of ϕ at Q_0, and $\eta = k\phi$. The helix is obtained as projection of a proper spiral wrapping the ellipsoid Σ modelling the AUT on the scanning cylinder via the hyperbolas at $\eta = \text{const}$ [8]. The parameter k is chosen such that the helix step, determined by two consecutive intersections with a given generatrix, is equal to the sample spacing $\Delta\eta = 2\pi/(2N'' + 1)$ needed for the interpolation along a generatrix, where $N'' = \text{Int}(\chi N') + 1$ and $N' = \text{Int}(\chi' W_\eta) + 1$. Accordingly, being $\Delta\eta = 2\pi k$, it follows that $k = 1/(2N'' + 1)$. The function $\text{Int}(x)$ gives the integer part of x and $\chi > 1$ is an oversampling factor needed to control the truncation error [3].

A nonredundant representation along the helix is then obtained by enforcing the optimal parameter ξ for describing it equal to β/W_ξ times the arclength of the projecting point on the spiral wrapping Σ and by choosing the related phase γ coincident with that ψ relevant to a generatrix. Moreover, the bandwidth W_ξ is chosen equal to β/π times the length of the spiral wrapping Σ from pole to pole [7, 8].

By exploiting these results, the voltage at P on the generatrix at

φ can be recovered via the following OSI expansion [8]:

$$\tilde{V}\left(\eta(\vartheta),\varphi\right)=\sum_{n=n_0-q+1}^{n_0+q}\tilde{V}\left(\eta_n\right)\Omega_N\left(\eta-\eta_n\right)D_{N''}\left(\eta-\eta_n\right) \tag{12}$$

wherein $\eta_n=\eta_n(\varphi)=\eta(\phi_s)+k\varphi+n\Delta\eta=\eta_0+n\Delta\,\eta$, $n_0=\mathrm{Int}[(\eta-\eta_0)/\Delta\eta]$, $2q$ is the number of retained samples, and

$$\begin{aligned} D_{N''}\left(\eta\right)&=\frac{\sin\left[\left(2N''+1\right)\eta/2\right]}{\left(2N''+1\right)\sin(\eta/2)};\\ \Omega_N\left(\eta\right)&=\frac{T_N\left[2\cos^2\left(\eta/2\right)/\cos^2\left(\bar{\eta}/2\right)-1\right]}{T_N\left[2/\cos^2\left(\bar{\eta}/2\right)-1\right]}\end{aligned} \tag{13}$$

are the Dirichlet and Tschebyscheff sampling functions [3], $T_N(\cdot)$ being the Tschebyscheff polynomial of degree $N=N''-N'$ and $\bar{\eta}=q\Delta\eta$.

The samples $\tilde{V}(\eta_n)$ could be retrieved [8] via an expansion along the helix, similar to (12), thus allowing the recovery of the voltage at any point on the cylinder. However, the proposed direct NF-FF transformation avoids the explicit interpolation of the nonredundant acquired data to recover those needed to carry out the classical NF-FF transformation with cylindrical scanning [20] or [22].

3. DIRECT NF-FF TRANSFORMATION

An efficient NF-FF transformation for evaluating the far field directly from the helicoidal NF data is described in this section. By taking into account the OSI expansion (12) and relation (7), the Fourier transforms (4) can be rewritten as:

$$\begin{aligned} I_\nu^{1,2}\left(\tau\right)=\sum_{n\in N_r}\int_0^{2\pi}\Bigg\{&\tilde{V}^{1,2}\left(\eta_n,\varphi\right)e^{-j\nu\varphi}\\ &\cdot\int_{-\infty}^{\infty}D_{N''}\left(\eta(z)-\eta_n\right)\,Q\left(\eta(z)-\eta_n\right)\,e^{-j\psi(z)}e^{j\tau z}dz\Bigg\}d\varphi\end{aligned} \tag{14}$$

where N_r is the set of indexes of all considered NF turns, $\tilde{V}^{1,2}(\eta_n,\varphi)$ are the samples of the reduced voltage at the intersection points between the generatrix at φ and the scanning helix, and $Q=\Omega_N$, if $|\eta(z)-\eta_n|\le q\Delta\eta$, or $Q=0$, otherwise.

The integration over z gives, for any fixed φ:

$$G_{n\tau}\left(\varphi\right)=\int_{z_i}^{z_f}D_{N''}\left(\eta(z)\,-\eta_n\right)\Omega_N\left(\eta(z)\,-\eta_n\right)e^{-j\psi(z)}e^{j\tau z}dz \tag{15}$$

where $z_i = z(\eta_n + q\Delta\eta)$ and $z_f = z(\eta_n - q\Delta\eta)$. Now, by substituting this last relation into (14), it results:

$$I_\nu^{1,2}(\tau) = \sum_{n\in N_r} \int_0^{2\pi} \tilde{V}^{1,2}(\eta_n, \varphi)\, G_{n\tau}(\varphi)\, e^{-j\nu\varphi} d\varphi \tag{16}$$

Such a relation involves an integration over φ that can be efficiently performed via the FFT algorithm, if the number of the voltage samples on each helix turn is always the same and equal to the smallest integer M_H, product of powers of 2, 3 and 5 equal or greater than $2[\mathrm{Int}(\chi'\beta\rho') + 1]$. In such a way, the samples lying on the helix at $\varphi_m = m\Delta\varphi = 2\pi m/M_H$ with $m = 0, \ldots, M_H - 1$ are all aligned. Accordingly, it results:

$$\begin{aligned} &\int_0^{2\pi} \tilde{V}^{1,2}(\eta_n, \varphi)\, G_{n\tau}(\varphi)\, e^{-j\nu\varphi} d\varphi \\ &= \frac{2\pi}{M_H} \sum_{m=0}^{M_H-1} \tilde{V}^{1,2}(\eta_{m,n}, \varphi_m)\, G_{n\tau}(\varphi_m) e^{-j\frac{2\pi m\nu}{M_H}} \end{aligned} \tag{17}$$

where

$$\eta_{m,n} = \eta_n(\varphi_m) = \eta(\phi_s) + k\varphi_m + n\Delta\eta \tag{18}$$

The summation can be efficiently performed via a direct FFT algorithm.

Note that the $G_{n\tau}(\varphi_m)$'s can be calculated (once and for all) for given sets of antennas, since they depend only on the measurement cylinder radius and on the AUT modelling. Moreover, from the efficiency viewpoint, it is convenient to employ this method to evaluate only the FF samples necessary to reconstruct the antenna pattern via the OSI expansion in [23], properly modified to deal with even numbers of samples along the meridians and parallels:

$$\begin{aligned} &F_{\vartheta,\varphi}(\vartheta(\eta), \varphi) \\ &= \frac{2N_F'' - 1}{2N_F''} \sum_{n=n_0-q+1}^{n_0+q} \left\{ \Omega_{N_F}(\eta - \eta_n) D_{N_F''-1}(\eta - \eta_n) \frac{2M_n'' - 1}{2M_n''} \right. \\ &\left. \cdot \sum_{m=m_0-p+1}^{m_0+p} F_{\vartheta,\varphi}(\eta_n, \varphi_{m,n}) \Omega_{M_n}(\varphi - \varphi_{m,n}) D_{M_n''-1}(\varphi - \varphi_{m,n}) \right\} \end{aligned} \tag{19}$$

wherein $n_0 = \mathrm{Int}[\eta/\Delta\eta]$, $m_0 = \mathrm{Int}[\varphi/\Delta\varphi_n]$, and

$$\eta_n = n\Delta\eta = n\pi/N_F''; \quad N_F'' = 2\left[\mathrm{Int}(\chi N'/2) + 1\right]; \quad N_F = N_F'' - N' \tag{20}$$

$$\varphi_{m,n} = m\Delta\varphi_n = m\pi/M_n''; \quad M_n'' = 2^i \geq \mathrm{Int}(\chi M_n') + 1;$$

$$M_n' = \mathrm{Int}\left[\chi^* \beta \sin\vartheta(\eta_n)\right] + 1 \tag{21}$$

$$M_n = M_n'' - M_n'; \quad \chi^* = 1 + (\chi' - 1)[\sin\vartheta(\eta_n)]^{-2/3} \tag{22}$$

The need of an OSI expansion tailored for an even number of samples along the parallels arises from the use of an efficient power of two FFT algorithm for computing (5) and (6). Whereas, N''_F has been chosen according to (20) in order to have FF samples on the equator. Obviously, there is no need to extract the phase factor from the far-field expression, since it is constant on the far-field sphere.

At last, it must be pointed out that the direct NF-FF transformation allows the reconstruction of the antenna far field in any cut plane at φ = constant and not only in those achievable by evaluating (5) and (6) via the FFT algorithm. Moreover, as shown in [19] and verified in the next section, it exhibits the very interesting feature to eliminate the ripple due to the discontinuity of the near field at the scanning zone edges.

4. NUMERICAL AND EXPERIMENTAL RESULTS

Some numerical and experimental results assessing the effectiveness of the proposed direct NF-FF transformation with helicoidal scanning are shown in this section.

The numerical simulation refers to a uniform planar array of elementary Huygens sources polarized along the z axis and covering an elliptical zone in the plane $y = 0$, with major and minor semi-axes equal to 12λ and 3λ. They are spaced by 0.5λ and 0.6λ along the x and z axes, respectively. An open-ended WR-90 rectangular waveguide, at the frequency of 10 GHz, is chosen as probe. The helix wraps a cylinder with radius $d = 10\lambda$ and height $h = 120\lambda$.

Figures 2 and 3 show the reconstruction of the antenna FF

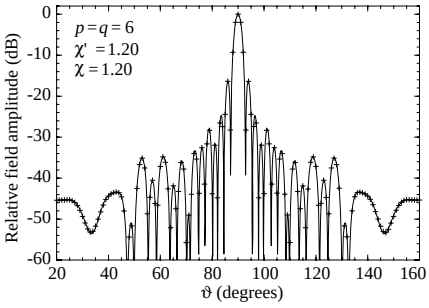

Figure 2. E-plane pattern. Solid line: exact. Crosses: reconstructed by means of the direct helicoidal NF-FF transformation.

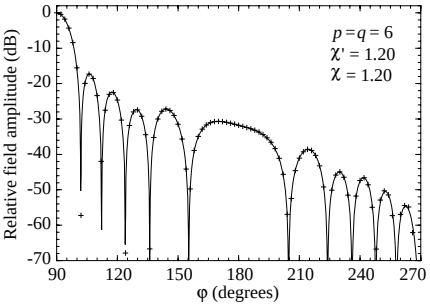

Figure 3. H-plane pattern. Solid line: exact. Crosses: reconstructed by means of the direct helicoidal NF-FF transformation.

pattern in the principal planes obtained by using the presented NF-FF transformation technique. As can be seen, the exact and reconstructed fields are practically indistinguishable, thus assessing the effectiveness of the approach. A further example relevant to the antenna FF pattern reconstruction in the plane at $\varphi = 60°$ is reported in Figure 4, in order to show the capability of the technique to accurately reconstruct the antenna far field in any cut plane.

It must be stressed that the number of used samples is 4 341, significantly less than that (14 460) required by the classical cylindrical NF-FF transformation [20] and by the helicoidal scanning technique [16] to cover the same scanning zone.

The experimental validation has been performed in the anechoic

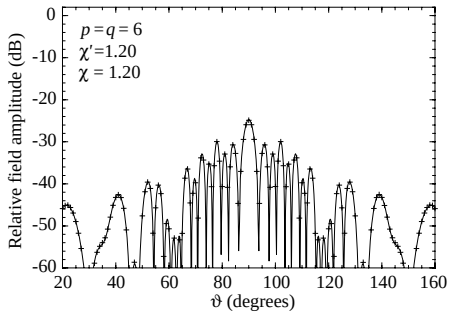

Figure 4. Far-field pattern in the plane at $\varphi = 60°$. Solid line: exact. Crosses: reconstructed by means of the direct helicoidal NF-FF transformation.

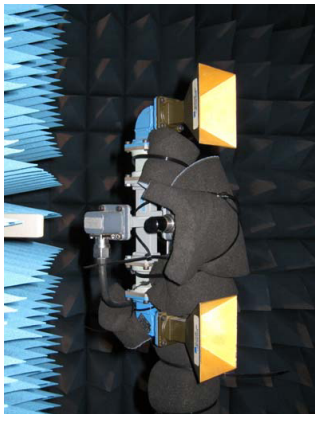

Figure 5. Photo of AUT 1.

chamber of the UNISA Antenna Characterization Lab, provided of an advanced cylindrical NF facility, supplied by MI Technologies. An open-ended WR90 rectangular waveguide is used as probe and its response has been collected on a cylinder with $d = 19.6\,\text{cm}$ and $h = 240\,\text{cm}$. The amplitude and phase measurements are carried out by means of a vectorial network analyzer. Two monopulse antennas, operating at 10 GHz in the sum mode, have been considered in the laboratory tests. They have been assembled using two pyramidal horns ($8.9 \times 6.8\,\text{cm}$), two straight and two curved rectangular waveguides, and a hybrid tee. In the former case (AUT 1), they are arranged to form a H-plane monopulse antenna (see Figure 5), wherein the distance between the two pyramidal horns centers is 26 cm. In the latter (AUT 2), an E-plane monopulse antenna is realized and the distance between the horns centers becomes 26.5 cm. Both the AUTs, located in the plane $y = 0$, have been modelled as enclosed in a prolate ellipsoid, having major and minor semi-axes equal to 24 cm and 6 cm, and 23.7 cm and 6.3 cm, respectively.

The FF pattern in the principal planes E and H reconstructed via the direct NF-FF transformation has been compared with that (reference) obtained by using the MI software from NF data measured on the classical cylindrical grid. In particular, Figures 6 and 7 refer to FF reconstructions when considering the AUT 1, whereas Figures 8 and 9 are relevant to those of AUT 2. As can be seen, a very good agreement results in both the cases, thus assessing the effectiveness of the technique.

It is worth noting that direct NF-FF transformation incorporates

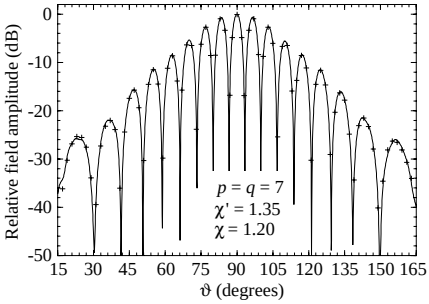

Figure 6. H-plane pattern (AUT 1). Solid line: reference. Crosses: reconstructed via the direct helicoidal NF-FF transformation.

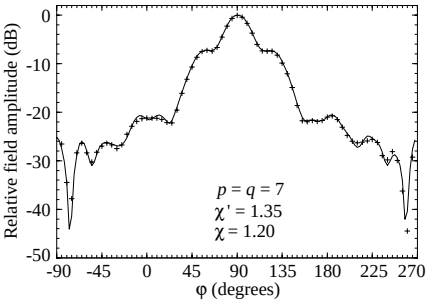

Figure 7. E-plane pattern (AUT 1). Solid line: reference. Crosses: reconstructed via the direct helicoidal NF-FF transformation.

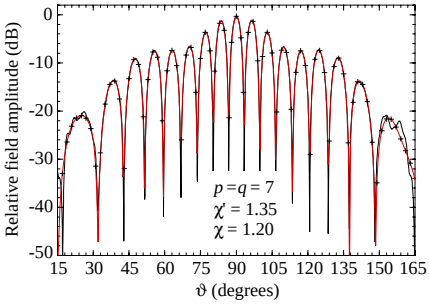

Figure 8. *E*-plane pattern (AUT 2). Solid line: reference. Red solid line with crosses: reconstructed via the direct helicoidal NF-FF transformation.

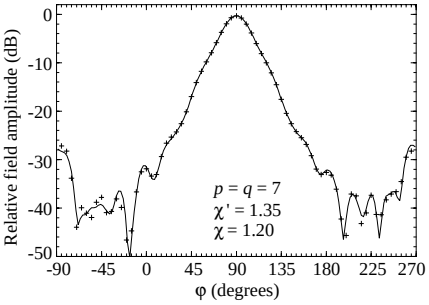

Figure 9. *H*-plane pattern (AUT 2). Solid line: reference. Crosses: reconstructed via the direct helicoidal NF-FF transformation.

the probe characterization and therefore it has been necessary to characterize [24] the employed probe according to [25], as done in the software package MI-3000 implementing the standard probe compensated NF-FF transformation [22], and verify that practically identical results are obtained when the same NF data are transformed by using the MI package or our version of the probe compensated NF-FF transformation [20].

It must be stressed that the proposed technique exhibits the particular property to eliminate the ripple caused by the discontinuity of the near field at the edges of the scanning surface (see Figure 8). Note that such an effect is now visible, since the near field level at the edge of the scanning cylinder is about 20 dB higher than for the AUT 1 case. Accordingly, the greater the amount of discontinuity at the edge of the scanning cylinder, the more visible the characteristic property of the direct helicoidal NF-FF transformation technique to eliminate the ripple.

Note that the number of used samples is 1 986 for the AUT 1 case and 2 202 for the AUT 2 one, significantly less than those (5 796 and 6 440) required by the MI software and by the helicoidal scanning technique [16] to cover the same scanning zone.

5. CONCLUSIONS

In this paper, an effective direct helicoidal NF-FF transformation for long antennas has been proposed and assessed both numerically and experimentally. It allows the antenna far field evaluation in any cut

plane directly from the helicoidal NF data without interpolating them and exhibits the interesting feature to eliminate the ripple caused by the discontinuity of the near field at the edges of the scanning surface. To simplify the mechanical scanning and to reduce the computational effort, a sampling arrangement different from that relevant to the rigorous application of the nonredundant sampling representation on the helix results. In particular, the number of the helix turns is fixed by the sampling representation using the prolate ellipsoidal modelling and the number of data on each of them according to the minimum cylinder rule, as in the classical cylindrical scanning.

REFERENCES

1. Bucci, O. M., C. Gennarelli, and C. Savarese, "Representation of electromagnetic fields over arbitrary surfaces by a finite and nonredundant number of samples," *IEEE Trans. Antennas Propagat.*, Vol. 46, 351–359, March 1998.
2. Bucci, O. M. and C. Gennarelli, "Application of nonredundant sampling representations of electromagnetic fields to NF-FF transformation techniques," *Int. Jour. of Antennas and Propagat.,* Vol. 2012, Article ID 319856, 14 pages, 2012.
3. Bucci, O. M., C. Gennarelli, and C. Savarese, "Fast and accurate near-field far-field transformation by sampling interpolation of plane-polar measurements," *IEEE Trans. Antennas Propagat.*, Vol. 39, 48–55, January 1991.
4. Yaccarino, R. G., L. I. Williams, and Y. Rahmat-Samii, "Linear spiral sampling for the bipolar planar antenna measurement technique," *IEEE Trans. Antennas Propagat.*, Vol. 44, 1049–1051, July 1996.
5. Bucci, O. M., C. Gennarelli, G. Riccio, and C. Savarese, "Nonredundant NF-FF transformation with helicoidal scanning," *Journal of Electromagnetic Waves and Applications*, Vol. 15, No. 11, 1507–1519, 2001.
6. D'Agostino, F., C. Gennarelli, G. Riccio, and C. Savarese, "Theoretical foundations of near-field-far-field transformations with spiral scannings," *Progress In Electromagnetics Research*, Vol. 61, 193–214, 2006.
7. D'Agostino, F., F. Ferrara, C. Gennarelli, R. Guerriero, and M. Migliozzi, "The unified theory of near-field-far-field transformations with spiral scannings for nonspherical antennas," *Progress In Electromagnetics Research B*, Vol. 14, 449–477, 2009.
8. D'Agostino, F., F. Ferrara, C. Gennarelli, R. Guerriero,

and M. Migliozzi, "Near-field-far-field transformation technique with helicoidal scanning for elongated antennas," *Progress In Electromagnetics Research B*, Vol. 4, 249–261, 2008.

9. D'Agostino, F., F. Ferrara, C. Gennarelli, R. Guerriero, and M. Migliozzi, "Laboratory tests assessing the effectiveness of the NF-FF transformation with helicoidal scanning for electrically long antennas," *Progress In Electromagnetics Research*, Vol. 98, 375–388, 2009.
10. D'Agostino, F., F. Ferrara, J. A. Fordham, C. Gennarelli, R. Guerriero, M. Mi-gliozzi, G. Riccio, and C. Rizzo, "An effective near-field-far-field transformation technique for elongated antennas using a fast helicoidal scan," *IEEE Antennas Propagat. Magazine*, Vol. 51, 134–141, August 2009.
11. Bucci, O. M., F. D'Agostino, C. Gennarelli, G. Riccio, and C. Savarese, "Probe compensated FF reconstruction by NF planar spiral scanning," *IEE Proc. — Microw., Antennas Propagat.*, Vol. 149, 119–123, April 2002.
12. D'Agostino, F., F. Ferrara, C. Gennarelli, R. Guerriero, and M. Migliozzi, "An effective NF-FF transformation technique with planar spiral scanning tailored for quasi-planar antennas," *IEEE Trans. Antennas Propagat.*, Vol. 56, 2981–2987, September 2008.
13. Bucci, O. M., F. D'Agostino, C. Gennarelli, G. Riccio, and C. Savarese, "NF-FF transformation with spherical spiral scanning," *IEEE Antennas Wireless Propagat. Lett.*, Vol. 2, 263–266, 2003.
14. D'Agostino, F., F. Ferrara, C. Gennarelli, R. Guerriero, M. Migliozzi, and G. Riccio, "A nonredundant near-field to far-field transformation with spherical spiral scanning for nonspherical antennas," *The Open Electrical & Electronic Eng. Jour.*, Vol. 3, 4–11, 2009.
15. D'Agostino, F., F. Ferrara, C. Gennarelli, R. Guerriero, and M. Migliozzi, "Far-field reconstruction from a minimum number of spherical spiral data using effective antenna modellings," *Progress In Electromagnetics Research B*, Vol. 37, 43–58, 2012.
16. Costanzo, S. and G. Di Massa, "Far-field reconstruction from phaseless near-field data on a cylindrical helix," *Journal of Electromagnetic Waves and Applications*, Vol. 18, No. 8, 1057–1071, 2004.
17. D'Agostino, F., F. Ferrara, C. Gennarelli, G. Riccio, and C. Savarese, "NF-FF transformation with cylindrical scanning from a minimum number of data," *Microw. Opt. Technol. Lett.*, Vol. 35, 264–270, November 2002.

18. D'Agostino, F., F. Ferrara, C. Gennarelli, G. Gennarelli, R. Guerriero, and M. Migliozzi, "Antenna pattern reconstruction directly from nonredundant near-field measurements collected by a cylindrical facility," *Progress In Electromagnetics Research M*, Vol. 24, 235–249, 2012.
19. D'Agostino, F., F. Ferrara, C. Gennarelli, R. Guerriero, and M. Migliozzi, "An innovative direct NF-FF transformation technique with helicoidal scanning," *Int. Jour. of Antennas and Propagat.,* Vol. 2012, Article ID 912948, 9 pages, 2012.
20. Leach, Jr., W. M. and D. T. Paris, "Probe compensated near-field measurements on a cylinder," *IEEE Trans. Antennas Propagat.,* Vol. 21, 435–445, July 1973.
21. Bucci, O. M., G. D'Elia, and M. D. Migliore, "Advanced field interpolation from plane-polar samples: Experimental verification," *IEEE Trans. Antennas Propagat.*, Vol. 46, 204–210, February 1998.
22. Yaghjian, A. D., "Near-field antenna measurement on a cylindrical surface: A source scattering matrix formulation," NBS Tech. note 696, U.S. Government Printing Office, Washington, DC, September 1977.
23. Bucci, O. M., F. D'Agostino, F. Ferrara, and C. Gennarelli, "Ellipsoidal source modellings for optimal far field interpolation," *Microw. and Opt. Technol. Lett.*, Vol. 29, 181–185, May 2001.
24. D'Agostino, F., F. Ferrara, C. Gennarelli, R. Guerriero, and M. Migliozzi, "On the direct nonredundant near-field-far-field transformation in a cylindrical scanning geometry," *IEEE Antennas Propagat. Magazine*, Vol. 54, 130–138, February 2012.
25. Yaghjian, A. D., "Approximate formulas for the far field and gain of open-ended rectangular waveguide," *IEEE Trans. Antennas Propagat.*, Vol. 34, 378–384, April 1984.